



Supplement of

Mid- and far-infrared spectral signatures of mineral dust from low- to high-latitude regions: significance and implications

Claudia Di Biagio et al.

Correspondence to: Claudia Di Biagio (claudia.dibiagio@lisa.ipsl.fr)

The copyright of individual parts of the supplement might differ from the article licence.

Figure S1. Raw absorbance spectra measured for the pure KBr pellets and for the replicates for Morocco, Niger and Bodélé samples.

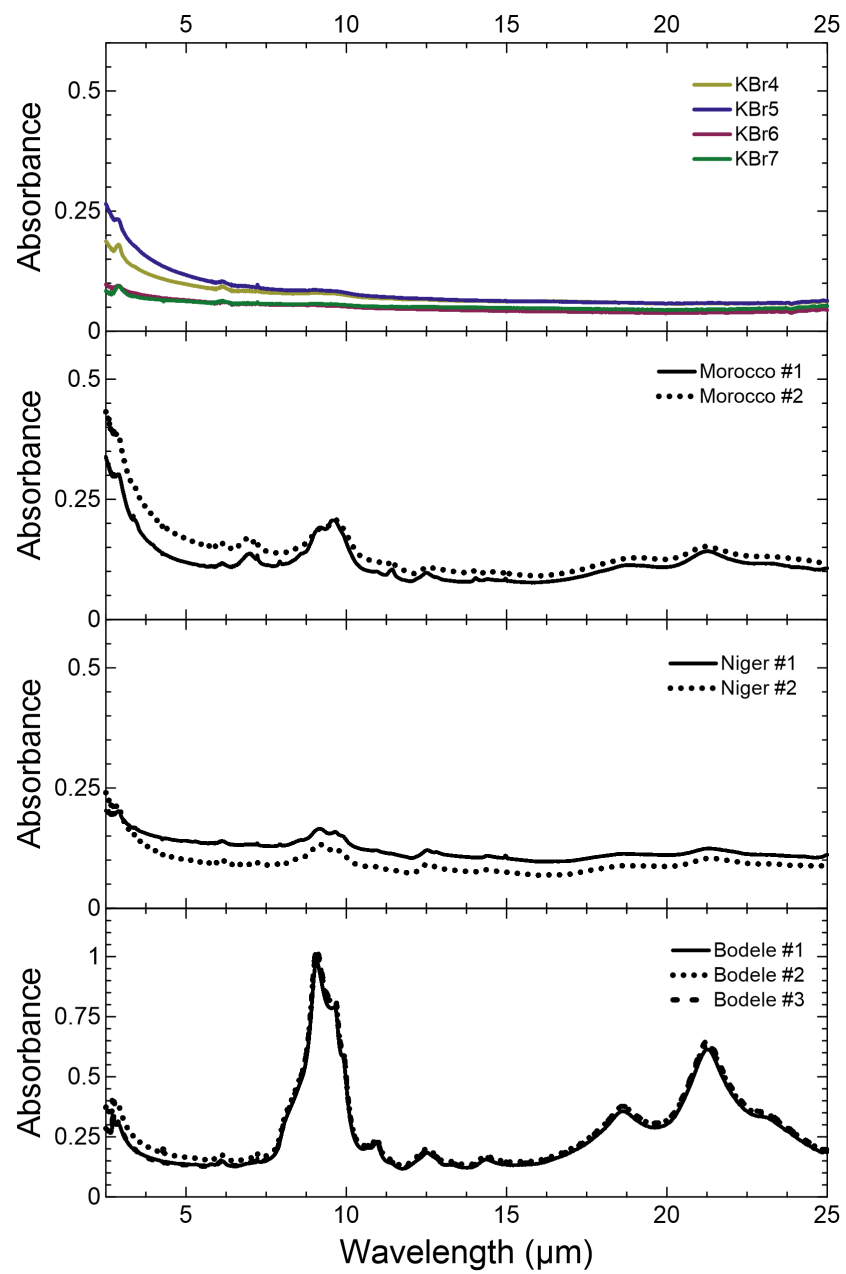


Figure S2. Raw absorbance spectra measured for the pure KBr pellets and for the replicates for Saudi Arabia, Kuwait, and Gobi samples.

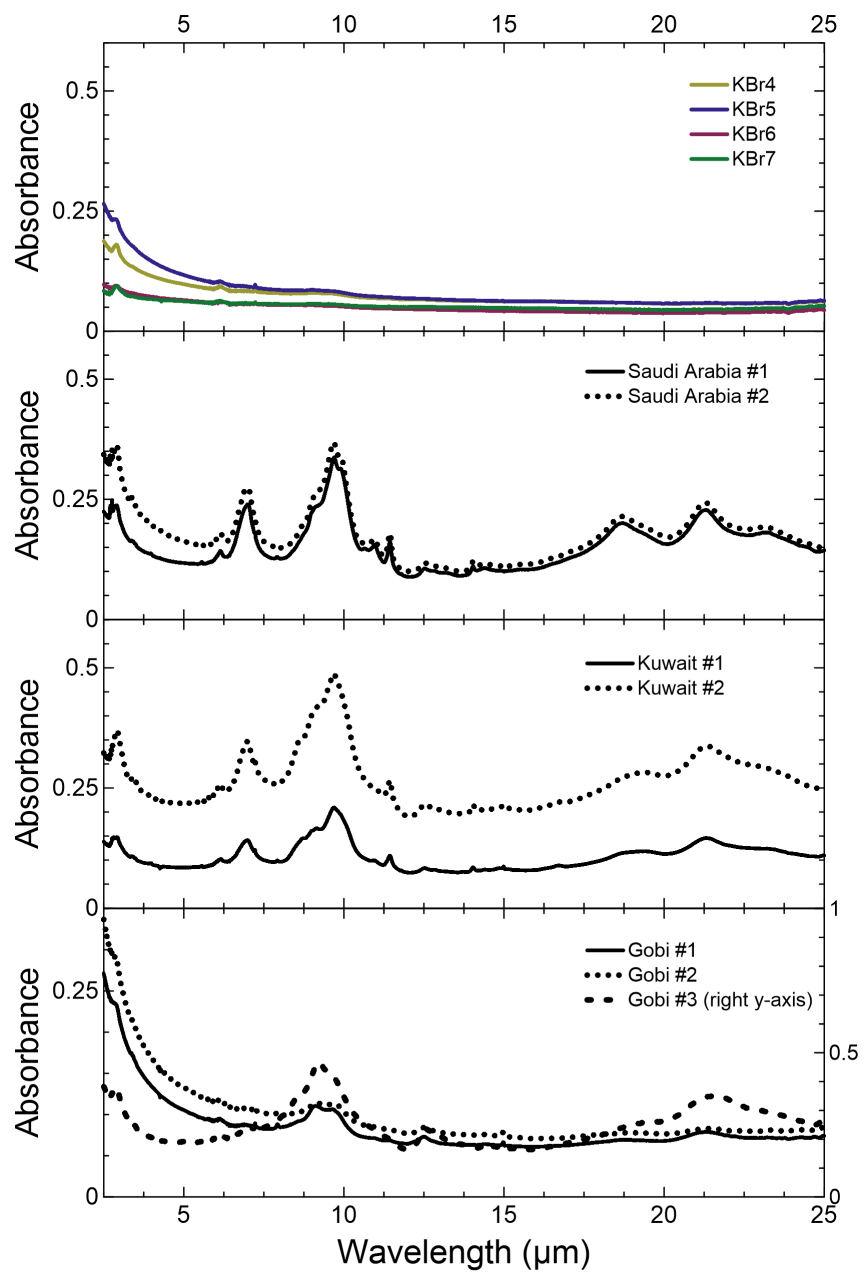


Figure S3. Raw absorbance spectra measured for the pure KBr pellets and for the replicates for Arizona and Atacama samples.

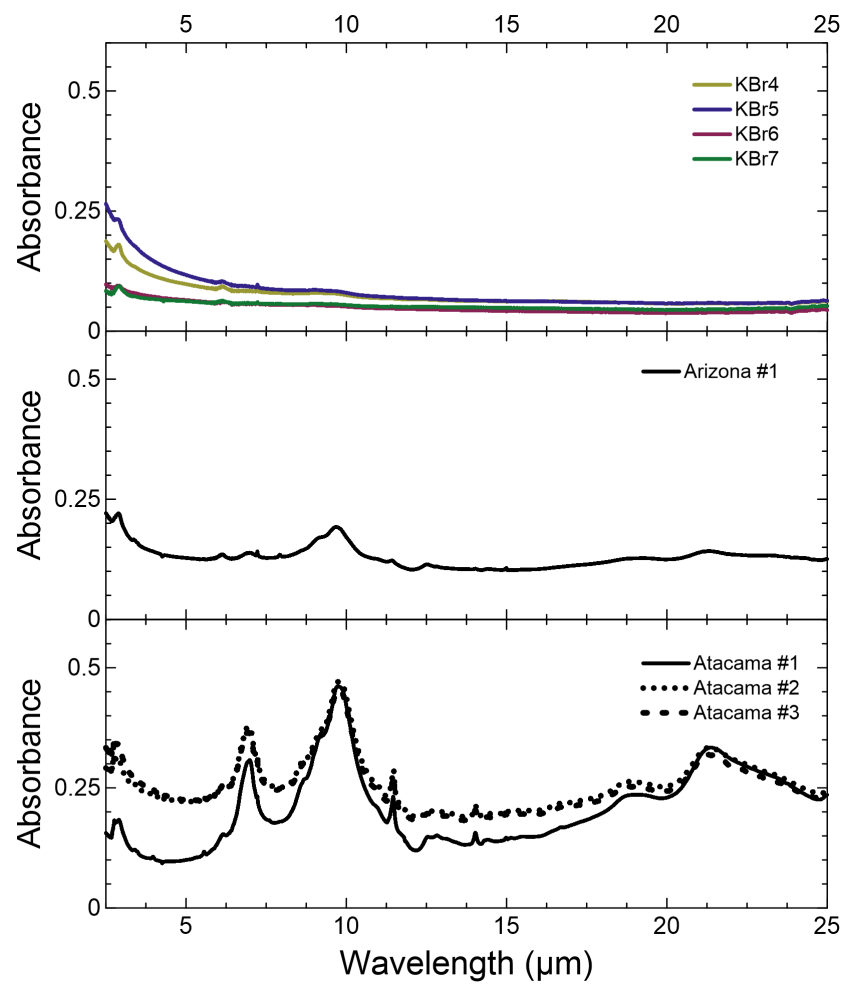


Figure S4. Raw absorbance spectra measured for the pure KBr pellets and for the replicates for Namib-1, Namib-H and Botswana samples.

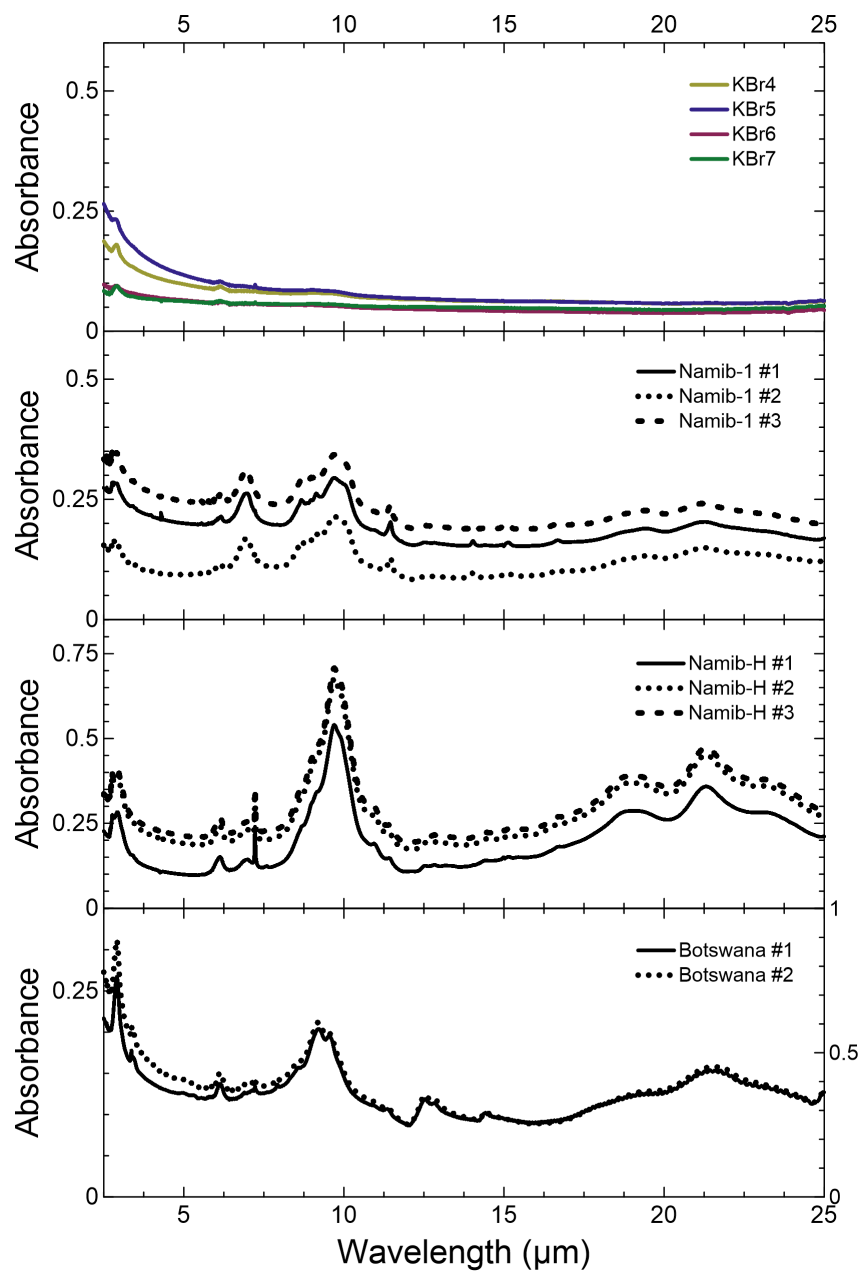


Figure S5. Raw absorbance spectra measured for the pure KBr pellets and for the replicates for Iceland-M and Iceland-H samples.

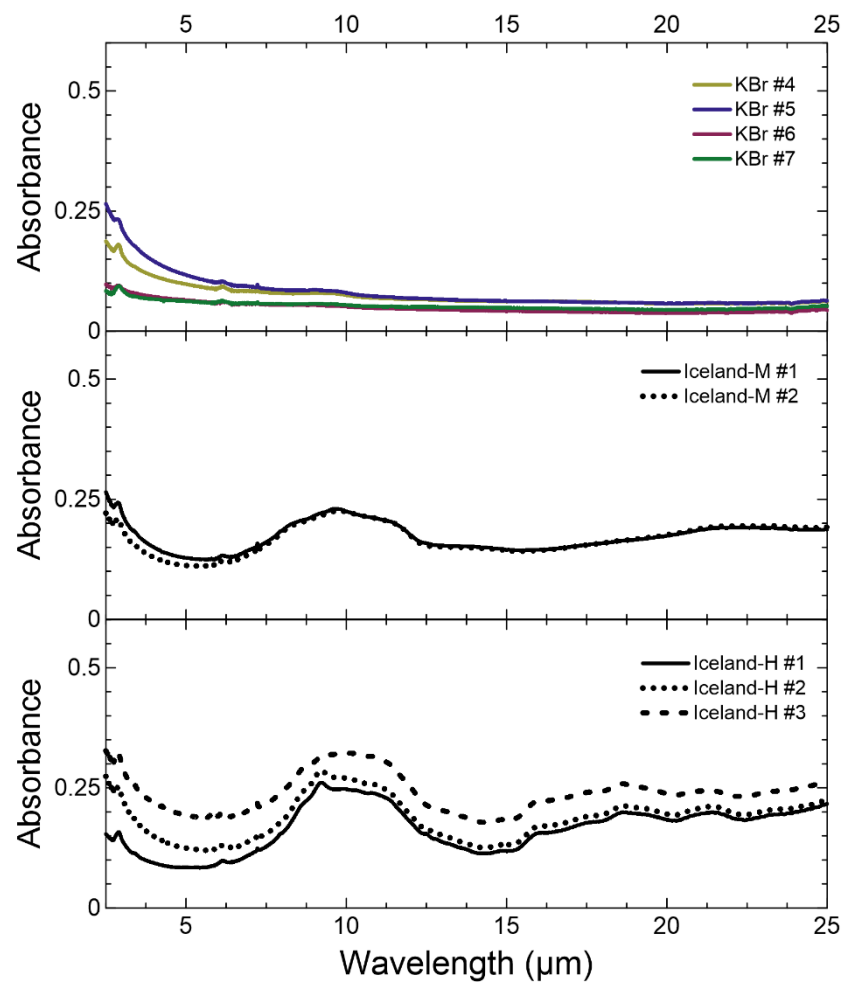


Figure S6. Comparison of the absorbance spectra obtained this study based on the pellet technique (blue line) and as measured in the CESAM chamber in Di Biagio et al. (2017) (red line). To facilitate the comparison, both the pellet and the chamber data are normalized so that the integral of the absorbance is 1 in the 8–15 μm spectral range.

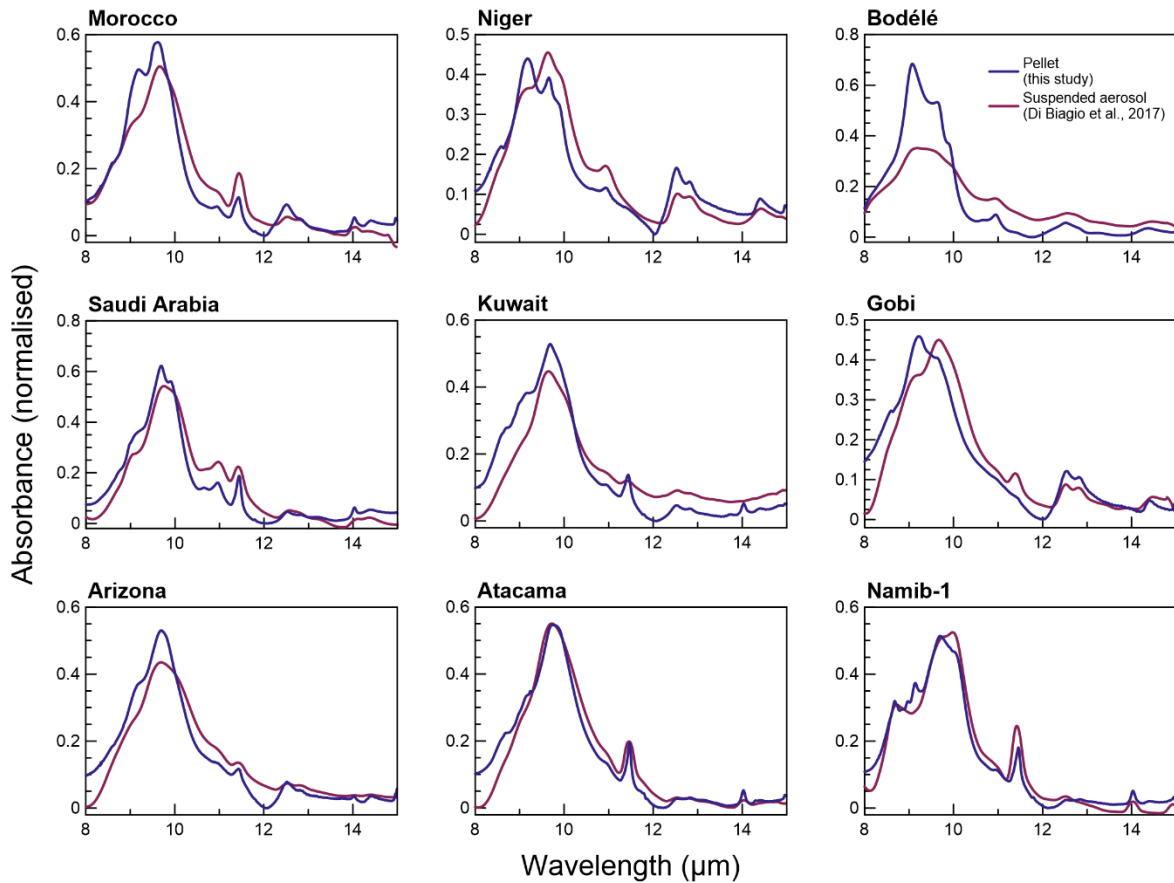


Figure S7. Absorbance spectra measured within the spectral range 2.5–25 μm for the thirteen different dust samples in this study. The Bodélé sample is plotted against the right y-axis. Each spectrum was corrected by subtracting the pure KBr spectrum that best fit the baseline of each dust-KBr pellet as detailed in Sect. 2.4 in the main manuscript.

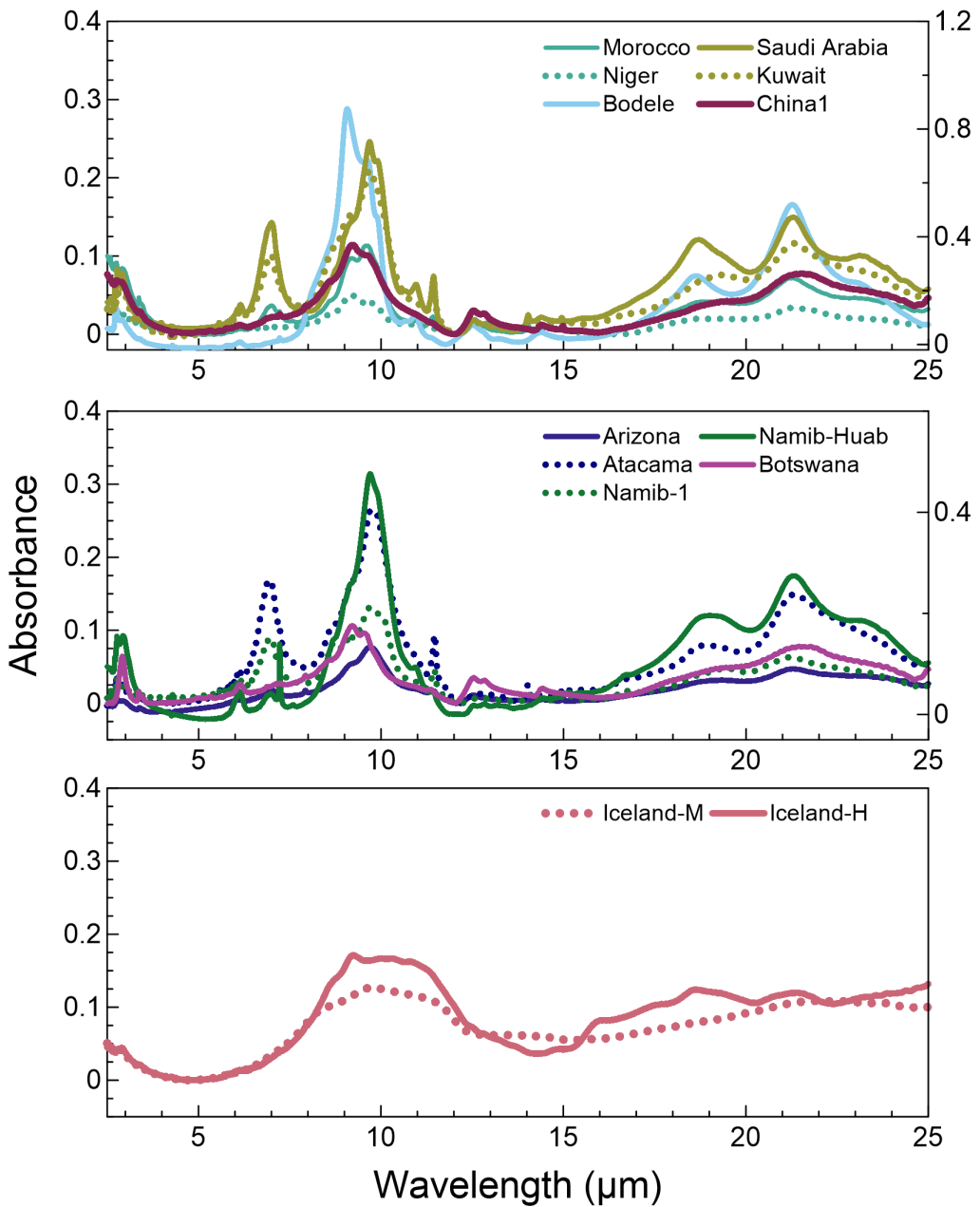


Figure S8. Comparison of the absorbance spectra obtained in this study for LMLD (blue lines) and Icelandic HLD (red lines) (normalized so that the integral of the absorbance is 1 in the 5-25 μm range) and the imaginary part of the complex refractive index obtained for natural dust aerosols based on pellet spectroscopic measurements up to 40 μm (Fouquart et al., 1987; Volz, 1972, 1973). The data correspond to rainout dust samples collected in Germany (Volz, 1972), Saharan dust from Barbados (Volz, 1973) and Niger dust (Fouquart et al., 1987).

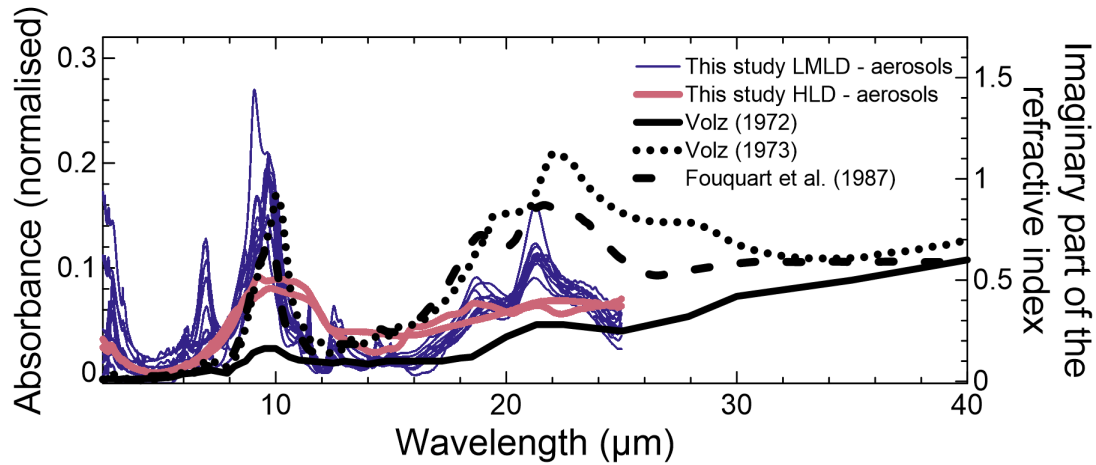


Table S1. Mineralogical composition (percentage by mass) of the dust aerosol samples analyzed in this study. Data for Morocco, Niger, Bodélé, Saudi Arabia, Kuwait, Gobi, Arizona, and Namib-1 are from Di Biagio et al. (2017). The estimated uncertainties associated with the identification of the different mineral species in (Di Biagio et al., 2017) are: clays $\pm 14\text{--}100\%$, quartz $\pm 9\%$, feldspars $\pm 8\text{--}14\%$, calcite $\pm 11\%$, dolomite $\pm 10\%$, gypsum $\pm 18\%$, iron oxides (goethite and hematite) $\pm 15\%$. Comparable uncertainties can be assumed for Namib-H and Botswana sample data. Data for Iceland-M (Myrdalssandur, MIR45 sample) and Iceland-H (Hagavatn, H55 sample) are from Baldo et al. (2020). Reported absolute uncertainties are 2.4 for glass, 2.3 for anorthite, 0.1 for augite and 0.1 for magnetite (Iceland-M) and 1.5 for glass, 1.7 for anorthite, 0.6 for microcline, 0.4 for augite, 0.3 for forsterite, and 0.1 for magnetite (Iceland-H).

Sample name	Amorphous	Phyllosilicates	Tectosilicates		Inosilicates	Nesosilicates	Carbonates		Iron oxides		
	Glass	Clays <i>Illite (I)</i> <i>Kaolinite (K)</i> <i>Chlorite (C)</i> <i>Palygorskite (P)</i> <i>Muscovite (Mu)</i>	Quartz	Feldspars <i>Orthoclase (O)</i> <i>Albite (A)</i> <i>Microcline (M)</i> <i>Anorthite (An)</i>	Pyroxene <i>Augite</i>	Olivine <i>Forsterite</i>	Calcite	Dolomite	Goethite	Hematite	Ti-Magnetite
Morocco		63.2 (38.4I 24.8K)	8.5	2.1 (O+A)			21.7	3.1	1.0	0.4	
Niger		51.2 (4.6I, 46.6K)	36.7	6.3 (O+A)					3.5	2.3	
Bodélé		53.5 (4.8I, 48.7K)	31.5	14.3 (O+A)						0.7	
Saudi Arabia		71.6	7.9	2.6 (O+A)			15.3		0.8	1.8	
Kuwait		56.7	25.0	14.8 (O+A)			2.0			1.5	
Gobi		45.5 (31.3I, 5.9K, 8.3 C)	27.0	7.9 (O+A)			18.7			0.9	
Arizona		63.1	18.9	10.1 (O+A)			6.4			1.5	
Atacama		69.4	10.5	6.1 (O+A)			12.4			1.6	
Namib-1		75.6	3.5	5.6 (O+A)			14.1		0.3	0.8	
Namib-H		60.0 (55.0I+P+Mu, 5.0K)	9.0	26.0 (A+M)			4.0			1.0	
Botswana		73.9 (42.9I+Mu, 31.0K)	26.1								
Iceland-M	91.3			3.5 (An)	3.6				0.2 (H+G)		1.4
Iceland-H	8.0			53 (10.2M, 2.8An)	29.3	7.2			0.5 (H+G)		2.0

Table S2. Information for single mineral data shown in Fig. 3 and 6 in the main manuscript. The table indicates the mineral name, the spectral range of data, the parameter (refractive index, absorbance), the source of data and the reference. Montmorillonite is taken as representative of the smectite family. Data for olivine are taken as representative for forsterite. No literature data are found for palygorskite and muscovite within the phyllosilicate family.

Mineral	Spectral range (μm)	Parameter	Source of data and/or data reference	Sample
Basaltic glass	0.4 – 50	CRI	(Pollack et al., 1973)	1- μm thick slab of basaltic glass
Kaolinite				
Illite				
Montmorillonite	5 – 100	CRI	(Glotch et al., 2007)	Fine powders of <2.0 or $<0.2 \mu\text{m}$ pressed in pellets
	8.1-11.9	Absorbance	(Dorschner et al., 1978)	KBr pellet
Chlorite	16.7 – 200	Absorbance	http://minerals.caltech.edu/FILES/Infrared_Far/Index.html	Polyethylene pellet
	0.8 – 36	CRI	(Spitzer and Kleinman, 1961)	Crystal
Quartz	16.7 – 200	Absorbance	http://minerals.caltech.edu/FILES/Infrared_Far/Index.html	Polyethylene pellet
Orthoclase	2.3-22.2	Absorbance	http://minerals.caltech.edu/FILES/Infrared_MIR/Minerals_From_JK/Index.htm	KBr pellet
Albite	2.5-13.5	Absorbance	(Laskina et al., 2012)	Suspended aerosol
Albite				
Anorthite				
Augite				
Forsterite				
Microcline	2.3-22.2	Absorbance	http://minerals.caltech.edu/FILES/Infrared_MIR/Minerals_From_JK/Index.htm	KBr pellet
Calcite	2.5 – 332	CRI	(Long et al., 1993)	Crystal
	2.5 – 40	CRI	(Querry, 1987)	Crystal
Dolomite	16.7 – 200	Absorbance	http://minerals.caltech.edu/FILES/Infrared_Far/Index.html	Polyethylene pellets
	0.1-1000	CRI	https://eodg.atm.ox.ac.uk/ARIA/ A.H.M.J. Triaud, private communication (2005), data from (Querry, 1985)	Crystal
Hematite	16.7 – 200	Absorbance	http://minerals.caltech.edu/FILES/Infrared_Far/Index.html	Polyethylene pellets
	8.3 – 50	CRI	(Glotch and Rossman, 2009)	Powder pellet
Goethite	16.7 – 200	Absorbance	http://minerals.caltech.edu/FILES/Infrared_Far/Index.html	Polyethylene pellets
Magnetite	0.2 – 55	CRI	https://refractiveindex.info/ (Polyanskiy, 2024), data from (Querry, 1985)	Crystal

Table S3. Main absorption peaks for the minerals composing dust in the range 2.5 to 100 μm based on published literature as listed in Table S1. Montmorillonite is taken as representative for the smectite family. No data are identified for palygorskite and muscovite. Data for olivine is taken as representative for forsterite. Data indicated with an asterisk are from absorbance spectra, while the others are from complex refractive index spectra.

Mineral	Absorption peak position (μm)
Basaltic glass ^a	9.5, 22
Kaolinite ^b	8.9, 9.7, 9.9, 10.6, 10.9, 12.6, 13.3, 14.6, 15.5, 16.6, 17.2, 17.9, 18.4, 18.7, 21.3, 23.2, 23.8, 24.4, 27, 28.8, 29.7, 31, 33, 36.2, 41.2, 44.2, 51.3, 54.3, 59.2, 64.1, 76.9, 83.3
Illite ^b	2.8, 6.2, 7, 8.6, 8.9, 9.2, 9.7, 10, 10.9, 11.4, 12, 12.5, 12.9, 13.3, 14.5, 15.7, 17.5, 18.8, 19.2, 21.2, 23.1, 23.8, 25.3, 26.9, 28.2, 30, 33.4, 38, 39.4, 51.8, 59.5, 75.2, 91.7
Montmorillonite ^b	6.1, 6.8, 8.5, 8.7, 8.9, 9.5, 9.6, 9.8, 10.9, 11.3, 11.8, 12.5, 14.1, 16.6, 18.1, 18.8, 19.2, 20.9, 21.4, 22, 23.3, 26.9, 29.1, 30.1, 31.3, 33.1, 36.1, 41.8, 50, 52.9
Chlorite ^c	9.2*, 10.4*, 21.6*, 22.8*, 27.3*
Quartz ^d	8.2, 8.6, 9.3, 12.5, 12.8, 14.3, 20.2, 22.2, 25.3, 27.4, 38.1*
Orthoclase ^e	8.8, 9.5, 9.9, 13, 13.8, 15.4, 16.5, 17.3, 18.7, 21.6
Albite ^{f,c}	8.7*, 9.1*, 9.7*, 17.0*, 18.9*, 21.7*, 24.0*, 26.7*, 30.0*, 36.5*, 40.0*, 46.0*, 50.0*, 54.0*, 61.0*, 68.2*
Anorthite ^e	17.8*, 18.7, 20.8*, 21.4*, 26.5*, 28.8*, 32.8*, 42.5*, 48.5*, 61.0*, 70.0*, 77.0*
Microcline ^e	12.5, 13.4, 14.8, 16, 16.8, 18.2, 20, 21.8
Augite ^e	19.7*, 21.4*, 25.3*, 30.5*, 34.8*, 41.5*, 70.0*
Forsterite ^e	19.9*, 24.3*, 28.2*, 34.8*
Calcite ^g	7, 11.5, 14.5, 33, 45.9
Dolomite ^{h,c}	6.4, 7, 11.4, 13.7, 28.5, 32.2, 38.5, 64.0*
Hematite ⁱ	18.8, 22.6, 33.5
Goethite ^{j,c}	17.9, 23.2, 29.1, 25.3*, 37.3*
Magnetite ^k	17.5, 28.6

^a (Pollack et al., 1973); ^b (Glotch et al., 2007); ^c http://minerals.caltech.edu/FILES/Infrared_Far/Index.html; ^d (Spitzer and Kleinman, 1961); ^e http://minerals.caltech.edu/FILES/Infrared_MIR/Minerals_From_JK/Index.htm; ^f (Laskina et al., 2012); ^g (Long et al., 1993); ^h (Querry, 1987); ⁱ <https://eodg.atm.ox.ac.uk/ARIA/>; A.H.M.J. Triaud, private communication (2005), data from (Querry, 1985); ^j (Glotch and Rossman, 2009); ^k (Querry, 1985) in (Polyanskiy, 2024)

Supplementary Text S1

Comparison of pellet and suspended LMLD absorbance spectra in the 8-15 μm spectral range

The comparison of the absorbance spectra for compressed pellet in the present study against suspended aerosols from the same LMLD source soils (Di Biagio et al., 2017) is shown in Fig. S7 for all common LMLD samples. The suspended aerosol data by Di Biagio et al. (2017) were obtained in the range 3-15 μm by means of in situ spectroscopy for aerosols generated with the same protocol of this study and suspended in the large CESAM simulation chamber (Chambre Expérimentale de Simulation Atmosphérique Multiphasique, (Wang et al., 2011)). Data for the comparison are restricted to the 8-15 μm range as below 8 μm the CESAM absorbance signal is contributed by scattering and so comparison with pellet measurements has a limited significance. The comparison in Fig. S7 suggests that the shape of the dust absorption in the 8-15 μm common spectral range is similar between pellets and suspended aerosols, but the quartz band at 9.3 μm seems overestimated in the pellet spectra, as identified in particular for Niger, Bodélé, Morocco, and Gobi. Indeed, the sample collection protocol described in Sect. 2.2 in the main manuscript implies that the re-suspended aerosol is collected in a glass vial directly out of the generation system. In this configuration it is possible that some grains of soil are entrained together with the aerosol and be therefore included in the pellet. As the soils are much richer in quartz than the aerosols (as also shown in Fig. 18 in Adebiyi et al. (2023) for the same LMLD samples of this work), the presence of few large soil grains can affect the quartz contribution to pellet spectra. This potential artefact however does not seem to influence the spectra in other regions within the 8-15 μm , supporting the idea of a limited impact to the main quartz bands (9.3, 12.5, 12.8, 20.2, 22.2 μm).

Supplementary Text S2

Detailed information on dust mineralogical composition analyses

The XRD measurements were carried out at the Université de Paris, Plateforme RX UFR – de Chimie, by means of a Panalytical Empyrean powder diffractometer equipped with Ni-filtered CuK_α radiation and operating at 45 kV and 40 mA.

In Di Biagio et al. (2017) the samples for XRD analyses were prepared based on the protocol by Caquineau et al. (1996) for dust collected on pycarbonate filters and low mass loadings (load deposited on filter $<800 \mu\text{g}$). Particles were deposited on a pure silicon slide and scanned from 5 to $60^\circ 2\theta$ range. Mass concentration of the non-clay phases (quartz, calcite, dolomite, gypsum, and feldspars) was retrieved by applying the semi-quantitative analysis (based on calibration curves established from reference minerals) following Klaver et al. (2011). The XRD measurements were complemented by X-ray Absorption Near-Edge Structure (XANES) analysis to derive iron oxide content and speciation in hematite and goethite, as described by Caponi et al. (2017). The mass concentration of clays (kaolinite, illite, smectite, palygorskite, chlorite) was not quantifiable from XRD spectra due to potential slight preferred orientation of the clays in the slide deposit and the absence of a proper reference material. The clay mass was estimated as the difference between the total dust mass obtained from complementary size and compositional measurements and the total mass of the identified XRD minerals and iron oxides. Clay speciation was estimated based on values of illite-to-kaolinite (I/K) and chlorite-to-kaolinite (Ch/I) mass ratios available in the literature for Northern African and Eastern Asian aerosols (Formenti et al., 2014; Scheuvens et al., 2013) and applied to Morocco, Niger, Bodèlè, and Gobi samples. For the other samples (Saudi Arabia, Kuwait, Arizona, Atacama, Namib-1) only the total clay mass was estimated.

For the other samples (Namib-H, Botswana, Iceland-M, Iceland-H) the XRD analysis was performed based on a more recent setup described by Nowak et al. (2018). This consisted in putting the sample into a borosilicate capillary that by rotation allows to see all the crystallographic orientations of the different mineral phases, therefore permitting to average the orientation-effect in the diffractograms. Data were recorded in the 3° - $70^\circ 2\theta$ range. The measurements were done in two steps in order to identify the mineral phases in the samples, and then quantify their content based on a Rietveld refinement procedure. The quantitative analysis of the XRD spectra was conducted with the MAUD (Material Analysis Using Diffraction) software to retrieve the amorphous and crystalline phases, including iron oxides. The reference mineral phase data used in the MAUD analysis were the ICSD-Pan (Inorganic Crystal Structure Database) and the COD (Crystallography Open Database) databases. As discussed by Baldo et al. (2020), the augite was chosen as reference for the amorphous phase for Icelandic dust. The iron oxides content in Icelandic dust samples and their speciation in hematite, goethite and magnetite was obtained by sequential extraction as described by Baldo et al. (2020).

Supplementary references

Adebiyi, A., Kok, J. F., Murray, B. J., Ryder, C. L., Stuut, J.-B. W., Kahn, R. A., Knippertz, P., Formenti, P., Mahowald, N. M., Pérez García-Pando, C., Klose, M., Ansmann, A., Samset, B. H., Ito, A., Balkanski, Y., Di Biagio, C., Romanias, M. N., Huang, Y., and Meng, J.: A review of coarse mineral dust in the Earth system, *Aeolian Research*, 60, 100849, <https://doi.org/10.1016/j.aeolia.2022.100849>, 2023.

Baldo, C., Formenti, P., Nowak, S., Chevaillier, S., Cazaunau, M., Pangui, E., Di Biagio, C., Doussin, J.-F., Ignatyev, K., Dagsson-Waldhauserova, P., Arnalds, O., MacKenzie, A. R., and Shi, Z.: Distinct chemical and mineralogical composition of Icelandic dust compared to northern African and Asian dust, *Atmospheric Chemistry and Physics*, 20, 13521–13539, <https://doi.org/10.5194/acp-20-13521-2020>, 2020.

Caponi, L., Formenti, P., Massabó, D., Di Biagio, C., Cazaunau, M., Pangui, E., Chevaillier, S., Landrot, G., Andreae, M. O., Kandler, K., Piketh, S., Saeed, T., Seibert, D., Williams, E., Balkanski, Y., Prati, P., and Doussin, J.-F.: Spectral- and size-resolved mass absorption efficiency of mineral dust aerosols in the shortwave spectrum: a simulation chamber study, *Atmospheric Chemistry and Physics*, 17, 7175–7191, <https://doi.org/10.5194/acp-17-7175-2017>, 2017.

Caquineau, S., Magonthier, M.-C., Gaudichet, A., and Gomes, L.: An improved procedure for the X-ray diffraction analysis of low-mass atmospheric dust samples, *European Journal of Mineralogy*, 9, 157–166, <https://doi.org/10.1127/ejm/9/1/0157>, 1996.

Di Biagio, C., Formenti, P., Balkanski, Y., Caponi, L., Cazaunau, M., Pangui, E., Journet, E., Nowak, S., Caquineau, S., Andreae, M. O., Kandler, K., Saeed, T., Piketh, S., Seibert, D., Williams, E., and Doussin, J.-F.: Global scale variability of the mineral dust long-wave refractive index: a new dataset of in situ measurements for climate modeling and remote sensing, *Atmospheric Chemistry and Physics*, 17, 1901–1929, <https://doi.org/10.5194/acp-17-1901-2017>, 2017.

Dorschner, J., Friedemann, C., and Görtler, J.: Laboratory spectra of phyllosilicates and the interstellar 10-micrometer absorption band, *Astronomische Nachrichten*, 299, 269–282, <https://doi.org/10.1002/asna.19782990602>, 1978.

Formenti, P., Caquineau, S., Desboeufs, K., Klaver, A., Chevaillier, S., Journet, E., and Rajot, J. L.: Mapping the physico-chemical properties of mineral dust in western Africa: mineralogical composition, *Atmospheric Chemistry and Physics*, 14, 10663–10686, <https://doi.org/10.5194/acp-14-10663-2014>, 2014.

Fouquart, Y., Bonnel, B., Brogniez, G., Buriez, J. C., Smith, L., Morcrette, J. J., and Cerf, A.: Observations of Saharan Aerosols: Results of ECLATS Field Experiment. Part II: Broadband Radiative Characteristics of the Aerosols and Vertical Radiative Flux Divergence, *Journal of Applied Meteorology and Climatology*, 26, 38–52, [https://doi.org/10.1175/1520-0450\(1987\)026%253C0038:OOSARO%253E2.0.CO;2](https://doi.org/10.1175/1520-0450(1987)026%253C0038:OOSARO%253E2.0.CO;2), 1987.

Glotch, T. D. and Rossman, G. R.: Mid-infrared reflectance spectra and optical constants of six iron oxide/oxyhydroxide phases, *Icarus*, 204, 663–671, <https://doi.org/10.1016/j.icarus.2009.07.024>, 2009.

Glotch, T. D., Rossman, G. R., and Aharonson, O.: Mid-infrared (5–100 μm) reflectance spectra and optical constants of ten phyllosilicate minerals, *Icarus*, 192, 605–622, <https://doi.org/10.1016/j.icarus.2007.07.002>, 2007.

Klaver, A., Formenti, P., Caquineau, S., Chevaillier, S., Ausset, P., Calzolai, G., Osborne, S., Johnson, B., Harrison, M., and Dubovik, O.: Physico-chemical and optical properties of Sahelian and Saharan mineral dust: in situ measurements during the GERBILS campaign, *Quarterly Journal of the Royal Meteorological Society*, 137, 1193–1210, <https://doi.org/10.1002/qj.889>, 2011.

Laskina, O., Young, M. A., Kleiber, P. D., and Grassian, V. H.: Infrared extinction spectra of mineral dust aerosol: Single components and complex mixtures, *Journal of Geophysical Research: Atmospheres*, 117, <https://doi.org/10.1029/2012JD017756>, 2012.

Long, L. L., Querry, M. R., Bell, R. J., and Alexander, R. W.: Optical properties of calcite and gypsum in crystalline and powdered form in the infrared and far-infrared, *Infrared Physics*, 34, 191–201, [https://doi.org/10.1016/0020-0891\(93\)90008-U](https://doi.org/10.1016/0020-0891(93)90008-U), 1993.

Nowak, S., Lafon, S., Caquineau, S., Journet, E., and Laurent, B.: Quantitative study of the mineralogical composition of mineral dust aerosols by X-ray diffraction, *Talanta*, 186, 133–139, <https://doi.org/10.1016/j.talanta.2018.03.059>, 2018.

Pollack, J. B., Toon, O. B., and Khare, B. N.: Optical properties of some terrestrial rocks and glasses, *Icarus*, 19, 372–389, [https://doi.org/10.1016/0019-1035\(73\)90115-2](https://doi.org/10.1016/0019-1035(73)90115-2), 1973.

Polyanskiy, M. N.: Refractiveindex.info database of optical constants, *Sci Data*, 11, 94, <https://doi.org/10.1038/s41597-023-02898-2>, 2024.

Querry, M. R.: Magnetite, Refractive index database, 1985.

Querry, M. R.: Optical constants of minerals and other materials from the millimeter to the UV, Aberdeen, MD, 1987.

Scheuvens, D., Schütz, L., Kandler, K., Ebert, M., and Weinbruch, S.: Bulk composition of northern African dust and its source sediments — A compilation, *Earth-Science Reviews*, 116, 170–194, <https://doi.org/10.1016/j.earscirev.2012.08.005>, 2013.

Spitzer, W. G. and Kleinman, D. A.: Infrared Lattice Bands of Quartz, *Phys. Rev.*, 121, 1324–1335, <https://doi.org/10.1103/PhysRev.121.1324>, 1961.

Volz, F. E.: Infrared Refractive Index of Atmospheric Aerosol Substances, *Appl. Opt.*, 11, 755–759, <https://doi.org/10.1364/AO.11.000755>, 1972.

Volz, F. E.: Infrared Optical Constants of Ammonium Sulfate, Sahara Dust, Volcanic Pumice, and Flyash, *Appl. Opt.*, 12, 564–568, <https://doi.org/10.1364/AO.12.000564>, 1973.

Wang, J., Doussin, J. F., Perrier, S., Perraudin, E., Katrib, Y., Pangui, E., and Picquet-Varrault, B.: Design of a new multi-phase experimental simulation chamber for atmospheric photosmog, aerosol and cloud chemistry research, *Atmospheric Measurement Techniques*, 4, 2465–2494, <https://doi.org/10.5194/amt-4-2465-2011>, 2011.